Phase diagram of a six-state chiral Potts model

H. Meyer* and J. C. Anglès d'Auriac*
Centre de Recherches sur les Très Basses Températures, BP 166, 38042 Grenoble, France
(Received 12 September 1994)

We present the two-dimensional phase diagram of an isotropic six-state chiral Potts model with a noncyclic Boltzmann weight matrix. This model has been introduced as being preintegrable in the sense that a very constraining functional relation for the partition function is known. The phase diagram shows itself to be very rich. In one region the model almost decouples, like a (q_s, q_t) model, in a product of two simpler models, while in another region a mean-field calculation gives good results compared to our Monte Carlo simulations. All the transition lines, as well as their order, are numerically determined. Besides, using the above-mentioned functional relation, an exact form for one of these transition lines is proposed. The low-energy states are also analyzed showing a variety of zero-temperature behavior in the different regions of the phase diagram.

I. INTRODUCTION

The q-state standard Potts model[1] is now universally recognized as an important model. It is indeed a good model for a variety of physical situations, but it is also a testing ground for different theories of classical physics on a lattice,[2] as well as for a variety of numerical methods.[3] Despite the fact that the partition function for $q > 2$ is only known at the critical temperature, the standard model is well understood.[2,4] To describe realistic situations many generalizations of the standard Potts model have been introduced. In particular, chiral Potts models have been proposed as being applicable to commensurate-incommensurate transition or floating phases (Ref. 5 and references quoted therein), the chirality being equivalent to a next-nearest neighbor interaction.[6] Another kind of useful generalization is provided by models having multicomponent dynamical variables. For example, the appearance of sinusoidally modulated phase in lipid bilayers was successfully modeled by a multicomponent $(3,2)$ system, where each site has both a two-state (Ising) variable and a three-state (Potts) variable.[7] Another example is provided by the description of the critical behavior of cubic rare-earth compounds by the same kind of two-component model.[8] At the same time much effort has been devoted to searching for new integrable generalized Potts models. The remarkable discovery of new solutions for the Yang-Baxter equations for one-component chiral Potts models triggered a number of publications in this field.[9–11] For example, the relationship between integrability and criticality has been studied both numerically and analytically.[12] New solutions of the star-triangle equations in multicomponent (N_α, N_β) models have been proposed.[13] Finally, the connection between multicomponent and one-component chiral Potts models has been studied.[14] Such a factorization of a one-component model into a multicomponent model has been found numerically in the present work.

Most of the known solutions of the Yang-Baxter equations concern models with *cyclic* Boltzmann weight matrices. The exact influence of this cyclicity is not yet clear. On the other hand, some exact results, using inversion relations,[15,4] were obtained for models where this cyclicity condition is not imposed.[16–19] These exact results concern, among others, a six-state chiral noncyclic Potts model denoted hereafter the Bellon-Maillard-Viallet (BMV) model. This six-state model is defined on a square lattice and depends on two sets of homogeneous variables, one set corresponding to the horizontal bonds and the other one corresponding to the vertical bonds. A functional relation for the partition function was shown to hold.[16] The aim of this paper is to present the complete phase diagram of the BMV model. We discuss the consequences of the functional relation for the partition function and give the results of extensive Monte Carlo simulations for an isotropic square lattice.

The paper is organized as follows: in the first part the model is presented in detail, together with a summary of the rigorous results available in the literature. In the second part the numerical methods are presented; the parameters and equilibrium criteria are also given. The two last parts discuss the results of the simulations and compare them with the exact results. The third part concerns the ferromagnetic region, while the fourth is devoted to the antiferromagnetic region and the mixed regions, where the physics is somewhat different.

II. SUMMARY OF EXACT RESULTS

An isotropic model with discrete spin variables on a square lattice with only nearest-neighbor interactions is defined by its Boltzmann weight matrix W. The partition function is

$$Z(\{W_{i,j}\}) = \sum_{\{\sigma\}} \prod_{\langle i,j \rangle} W_{\sigma_i,\sigma_j} , \tag{2.1}$$

where $\sigma_i \in Z_q$. The sum of the right-hand side runs over the q^N configurations ($N = L \times L$ is the number of sites) and the product runs over all the bonds $\langle i,j \rangle$

of the square lattice. For the BMV model (denoted $\mathbf{P_3}$ in Refs. 16 and 17) we have $q = 6$ and the following noncyclic Boltzmann weight matrix:

$$W = \begin{pmatrix} x & y & z & y & z & z \\ z & x & y & z & y & z \\ y & z & x & z & z & y \\ y & z & z & x & z & y \\ z & y & z & y & x & z \\ z & z & y & z & y & x \end{pmatrix} \equiv \begin{pmatrix} A(x,y,z) & B(y,z) \\ B(y,z) & A^t(x,y,z) \end{pmatrix} , \tag{2.2}$$

where

$$A(x,y,z) = \begin{pmatrix} x & y & z \\ z & x & y \\ y & z & x \end{pmatrix} , \quad B(y,z) = \begin{pmatrix} y & z & z \\ z & y & z \\ z & z & y \end{pmatrix} . \tag{2.3}$$

The matrix W depends on three homogeneous variables, x, y, and z. As in Ref. 16 we will use the two independent parameters, $u = y/x$ and $v = z/x$. Since the matrix W is *not* symmetric, we have to give an arbitrary orientation to the lattice: for example, we can choose to put arrows from the left to the right on the horizontal bonds and to put arrows from the top to the bottom on the vertical bonds. Note that the matrix (2.2) does not enter exactly in the scheme of the multicomponent Potts models for which solutions of the star-triangle relations are known[13,14] because the submatrix A is repeated in its transposed form, but matrix W exhibits the remarkable property of being stable with respect to matrix inversion. This property can be used to deduce a relation obeyed by the transfer matrix and consequently by the partition function.[15–20] This has been the motivation for the present work.

Using this relation together with the $\pi/2$ rotational invariance of the model it was shown in Ref. 16 that the partition function of the anisotropic model verifies the following relation:

$$Z((u,v),(\bar{u},\bar{v})) = \frac{\varphi(\bar{u},\bar{v})}{\varphi(J(u,v))} Z(IJ(u,v), JI(\bar{u},\bar{v})) , \tag{2.4}$$

where

$$\varphi(u,v) = [(1-u)(1-v)(1+2u+3v)]^L , \tag{2.5}$$

$$I(u,v) = \left(\frac{-u^2-u+2v^2}{1+u+2v-u^2-2uv-v^2}, \frac{u^2+vu-v^2-v}{1+u+2v-u^2-2uv-v^2} \right) , \tag{2.6}$$

$$J(u,v) = (1/u, 1/v) . \tag{2.7}$$

Here $u = y/x$ and $v = z/x$ refer to horizontal bonds, while $\bar{u} = \bar{y}/\bar{x}$ and $\bar{v} = \bar{z}/\bar{x}$ refer to vertical bonds. The form (2.4) allows us to discuss the isotropic case, although the mapping (IJ, JI) does not preserve the isotropy; this means that applying the transformation (IJ, JI) to an isotropic point (u,v,u,v) generally does not give an isotropic point $(u',v',u'' \neq u', v'' \neq v')$. The two involutions I and J generate an infinite discrete group of birational transformations. The algebraic expression,

$$\Delta(u,v) = \frac{(2v^2+2vu-u^2-2u^3-2vu^2+v^2u)(u-v^2)^2}{(v+u)^4(1-u)(1-v)^2} , \tag{2.8}$$

is invariant under the action of the elements of this infinite group. The orbits $\Delta(u,v) = \delta$ are generically elliptic curves, which foliate the phase diagram, but for some values of δ these orbits become rational curves. For example, $\Delta(u,v) = 3/16$ gives the standard Potts model. For other values of δ the previous group generated by I and J degenerates into a group of finite order. For example, $\delta = 0$ corresponds to the two branches $u = v^2$ for which $(IJ)^3(u,v) = (u,v)$ and

$$2u^2 + 2uv - 2u^3 - 2vu^2 + v^2u = 0 , \tag{2.9}$$

for which $(IJ)^6(u,v) = (u,v)$. As explained in Ref. 20 there is no Kramers-Wannier (geometrical) duality on this model, but the collineation

$$C_0(u,v) = \left(\frac{1-u}{1+2u+3v}, \frac{1-v}{1+2u+3v} \right) \tag{2.10}$$

can be seen as a generalization of the Kramers-Wannier duality.[21] The line

$$\Delta : \ 2u+3v = \sqrt{6}-1 \tag{2.11}$$

is invariant under C_0. We call it a self-dual line. It is shown in Fig. 2. Point B is the point where the self-dual line Δ intersects the curve (2.9), where the symmetry group degenerates into a finite group of order 6. This point of enhanced symmetry turns out to play a special role in the phase diagram as explained below in Sec. IV. The coordinates of the point B are (0.371 88,0.235 24).[20]

We can generalize a perturbation argument due to Kardar[22] to the BMV model, which works as follows: The element W_{σ_i,σ_j} of the matrix (2.2) can be rewritten as

$$W_{\sigma_i,\sigma_j}(u,v) = v^{1-\delta_{\sigma_i,\sigma_j}} \left(1 + \frac{u-v}{v} U_{\sigma_i,\sigma_j} \right) , \tag{2.12}$$

where $\delta_{\sigma_i,\sigma_j}$ is the Kronecker symbol, and the matrix U is given by

$$U = \begin{pmatrix} 0 & 1 & 0 & 1 & 0 & 0 \\ 0 & 0 & 1 & 0 & 1 & 0 \\ 1 & 0 & 0 & 0 & 0 & 1 \\ 1 & 0 & 0 & 0 & 0 & 1 \\ 0 & 1 & 0 & 1 & 0 & 0 \\ 0 & 0 & 1 & 0 & 1 & 0 \end{pmatrix} . \quad (2.13)$$

The term $v^{1-\delta_{\sigma_i,\sigma_j}}$ in (2.12) corresponds to a standard Potts model with v as the Boltzmann weight for a bond between two spins of *different* colors. We note that $Z'(v)$ is the partition function of this modified standard Potts model. It follows that

$$Z(u,v) = Z'(v) \left\langle \prod_{\langle i,j \rangle} \left(1 + \frac{u-v}{v} U_{\sigma_i,\sigma_j} \right) \right\rangle , \quad (2.14)$$

where the average $\langle\ \rangle$ is the thermodynamic average for the modified standard Potts model with Boltzmann weight v. Suppose now that we are in the vicinity of the standard Potts model, so that $(u-v)/v$ is a small parameter. We develop the product, and, to first order in $(u-v)/v$, we find

$$Z(u,v) = Z'(v) \left(1 + \frac{u-v}{v} \sum_{\langle i,j \rangle} \langle U_{\sigma_i,\sigma_j} \rangle \right) , \quad (2.15)$$

but, since the standard Potts model is insensitive to different colors, we have for the average $\langle U_{\sigma_i,\sigma_j} \rangle$

$$\langle U_{\sigma_i,\sigma_j} \rangle = \frac{2}{5} \langle 1 - \delta_{\sigma_i,\sigma_j} \rangle . \quad (2.16)$$

Finally we see that, to first order in $(u-v)/v$ the partition function $Z(u,v)$ of the BMV model can approximately be expressed by the partition function Z' of the modified standard Potts model:

$$Z(u,v) \approx Z' \left(\frac{2u+3v}{5} \right) . \quad (2.17)$$

Therefore the transition point $P : u = v = 1/(\sqrt{6}+1)$ is not an isolated point. The modified standard Potts model undergoes a phase transition when the argument of its partition function Z' equals $1/(\sqrt{6}+1)$. With the expression from Eq. (2.17) this yields exactly the self-dual line (2.11). So there is a line of first-order transition points intersecting the $u = v$ standard Potts line at the usual transition point P with a slope of $-2/3$.

To conclude this section, we introduce the BMV model on a Bethe lattice as a mean-field approximation. We direct the arrows on each bond towards the root. The matrix (2.2) has the property that $\sum_{\sigma_i=0}^{5} W_{\sigma_i,\sigma_j}$ is independent of σ_j. It is therefore straightforward to see that the partition function of the BMV model on a Bethe lattice is $Z_B(u,v) = (1+2u+3v)^M$ where M is the number of bonds. The internal energy and the specific heat can be easily deduced. We will see in Sec. V that this independent bond model is a surprisingly good approximation of the BMV model on a square lattice in some regions of the phase diagram.

III. NUMERICAL METHOD

To investigate the different regions of the phase diagram of the isotropic BMV model we have performed extensive Monte Carlo simulations. We used the usual heat-bath algorithm, which is very appropriate for chiral multistate models including antiferromagnetic bonds.[3] The use of a powerful parallel twelve processor computer allowed us to perform as many as 10^{10} Monte Carlo steps per spin (MCS/spin) for all the simulations of this work. The equilibrium was checked comparing two determinations of the specific heat, the one being a numerical differentiation of the internal energy with respect to temperature and the other one being the fluctuations of the internal energy divided by the square of the temperature. Using this criterion we had typically to perform 10^4 MCS/spin to reach the equilibrium from a random configuration (transient regime) and to average more than 10^6 values for a 128×128 periodic square lattice. The phase diagram is plotted in the (u,v) plane. However, to check equilibrium and for the interpretation of the results we need to have the thermodynamic quantities as functions of temperature. So we used a different parametrization and defined an asymmetry ρ and the temperature T by the following equations:

$$u = \exp\left(\frac{-\rho}{T}\right), \quad v = \exp\left(\frac{-1}{T}\right)$$

This amounts to having three types of bonds. For the type x bonds with Boltzmann weight x [see Eq. (2.2)] the coupling energy is $J_x = 0$. For the type y bonds with Boltzmann weight y this energy is $J_y = -\rho$, and for the type z bonds with Boltzmann weight z this energy is $J_z = -1$. In Fig. 1 some iso-ρ lines are shown. In particular the value $\rho = 1$ represents the standard Potts model. Figure 2 represents the phase diagram. Note that, to make the diagram more readable, we have plotted on the horizontal axis the variable u when $0 \le u \le 1$ and the variable $1/u$ when $u > 1$. Similarly the variable on the vertical axis is v when $0 \le v \le 1$ and $1/v$ when $v > 1$.

The energy of a configuration is completely determined by the two numbers n_y of bonds of type y and n_z of bonds

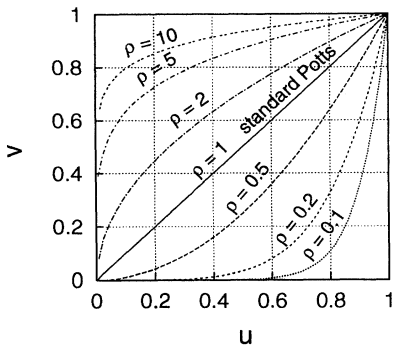

FIG. 1. Some lines of constant asymmetry ρ in the ferromagnetic region of the phase diagram. The point $u = v = 1$ corresponds to ∞ temperature and the origin to zero temperature.

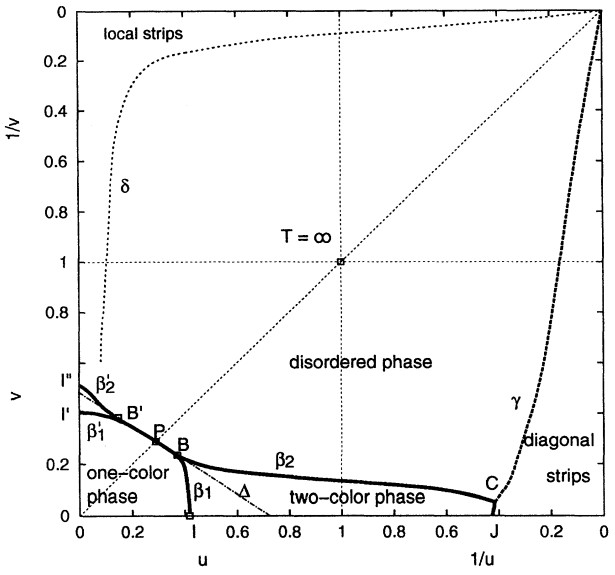

FIG. 2. The phase diagram of the BMV model (see text).

of type z, since n_x, n_y and n_z add up to the fixed total number of bonds. The full energy distribution is then *two* dimensional. The usual histogram method[23,3] can be generalized to extrapolate from a point (ρ, T) in the phase diagram to another point (ρ', T'). One has

$$P_{K'}(E) = \frac{e^{(K'-K)E}}{\sum_E P_K(E) e^{(K'-K)E}} P_K(E) ,$$

where $K = (-\rho/T, -1/T)$, and $E = (n_y, n_z)$, and the product KE is the scalar product. For each simulation point, we have recorded the full two-dimensional distribution of the energy, and we have extrapolated it to other

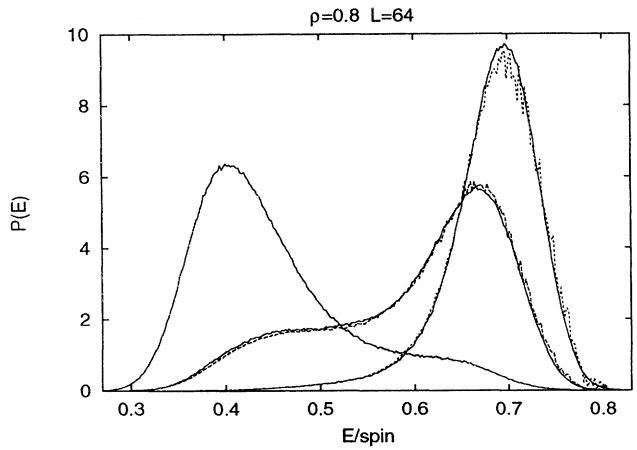

FIG. 3. The energy distribution for an asymmetry $\rho = 0.8$ for three different temperatures. The full lines are the distribution taken from the simulations at temperature $T_1 = 0.736$, $T_2 = 0.738$, and $T_3 = 0.740$. The two dotted lines are the extrapolations of the distribution for T_1, respectively, to T_2 and T_3.

close temperature values keeping the asymmetry ρ constant. From the energy distribution it is straightforward to compute the specific heat. When a point for a temperature, say T, was not obtained from a direct simulation but from extrapolation, we required two extrapolations, the one from a higher temperature and the other from a lower temperature, to agree. An example of such extrapolations is shown in Fig. 3. This closes the description of the technical details of the algorithm, and we turn now to the results.

IV. FERROMAGNETIC REGION

In the domain $0 \leq u \leq 1$ and $0 \leq v \leq 1$ the configurations with all the spins having the same color are of lowest energy. We therefore call it the ferromagnetic region. The standard Potts model characterized by $u = v$ or, equivalently, $\rho = 1$ belongs to this region.

We first focus on the lower triangle $0 \leq v \leq u \leq 1$. Figure 4 shows the typical behavior for two different values of the asymmetry, for $\rho = 0.8$ and $\rho = 0.5$. The specific heat as a function of temperature presents for $\rho = 0.8$ one single maximum, which becomes sharper when the size increases. This is the same behavior as that of the standard Potts model ($\rho = 1$). This maximum signals the occurrence of a phase transition in the thermodynamic limit. Using a finite-size scaling analysis, we have located the transition temperature. The one-dimensional probability distribution of the energy near the transition temperature is depicted in Fig. 5, where the distribution corresponding to $\rho = 0.8$ is the solid line. This probability distribution is clearly bimodal showing the coexistence of two phases, and the transition is therefore a first-order transition. When the asymmetry ρ is smaller, the behavior is completely different. The specific heat for $\rho = 0.5$ is shown on Fig. 4. The presence of two maxima suggests the existence of two transitions. The energy probability distribution for each of the two corresponding temperatures is unimodal, and therefore we suppose a second-order phase transition in both cases. We then have performed several simulations for other values of the asymmetry in order to locate the transition points as well as the order of these transitions. We found that the line Δ [Eq. (2.11)] is precisely a line of first-order transition up to the point of enhanced symmetry B introduced in Sec. II. The transition line then splits into two second-order lines. One of these two lines (line β_2 in Fig. 2) will extend into the nonferromagnetic region, while the other one (line β_1 in Fig. 2) ends at point I. Note that this point I is obtained assuming that for $v = 0$ the model *exactly* reduces to an Ising model and taking the exact Onsager value for T_c (for $v = 0$ the Markov chain generated by the Metropolis method is not ergodic any longer, and the algorithm breaks down). The two order parameters were identified to be

$$m_I = \frac{1}{L^2} \sum_i \left| (\delta_{\sigma_i,0} + \delta_{\sigma_i,1} + \delta_{\sigma_i,2}) - (\delta_{\sigma_i,3} + \delta_{\sigma_i,4} + \delta_{\sigma_i,5}) \right| , \quad (4.1)$$

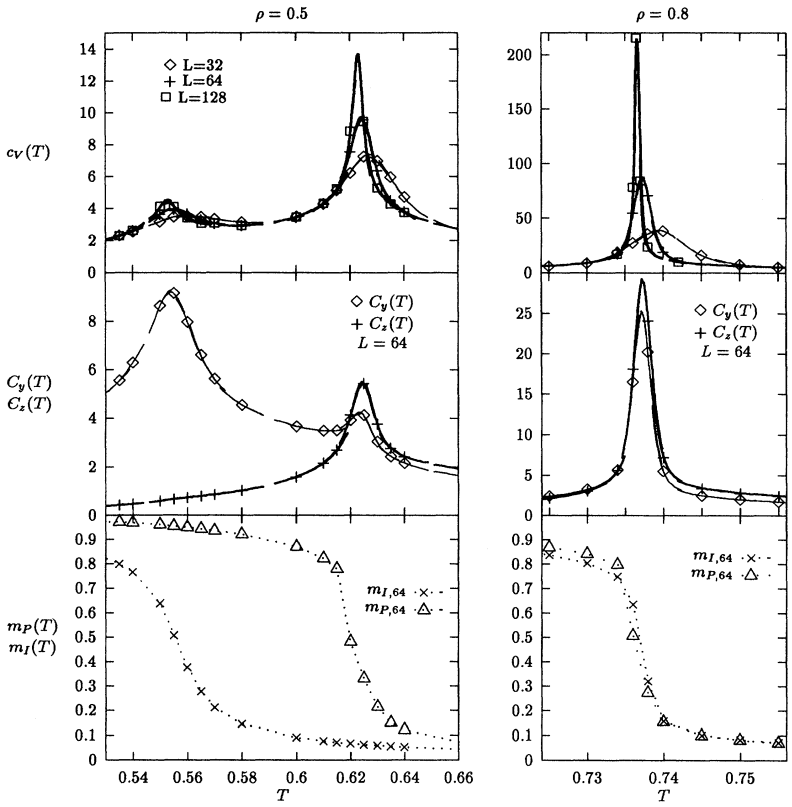

FIG. 4. Specific heat, fluctuations of the quantities n_y and n_z, and the order parameters as functions of the temperature for $\rho = 0.5$ and $\rho = 0.8$ (see text). Lines are obtained extrapolating with the help of the histogram method, execpt for the order parameters, where they are only guides to the eyes.

$$m_P = \frac{1}{L^2} \sum_i \left| (\delta_{\sigma_i,0} + \delta_{\sigma_i,3}) - (\delta_{\sigma_i,2} + \delta_{\sigma_i,5}) \right| . \quad (4.2)$$

The intuitive idea behind these parameters is the following. For high temperature the partition function is invariant under any permutation of the six colors, and we have $m_I = 0$ and $m_P = 0$. For intermediary values of the temperature the full symmetry is broken and only the exchange of two colors of a difference of three $(0-3, 1-4, 2-5)$ leaves the system invariant. The system is then in a two-color phase, and we have $m_I = 0$ and $m_P > 0$. Finally for low enough temperature one recovers a one-color ferromagnetic phase where $m_I > 0$ and $m_P > 0$. According to this idea the high-temperature branch β_2 should be of the same universality class as the $q = 3$ standard Potts model, and the low-temperature branch β_1 should be of the Ising universality class. We have succesfully tested this hypothesis, performing finite-size scaling analysis for each of the transitions and for different values of the asymmetry. The results are summarized in Table I, which gives the values of the exponent

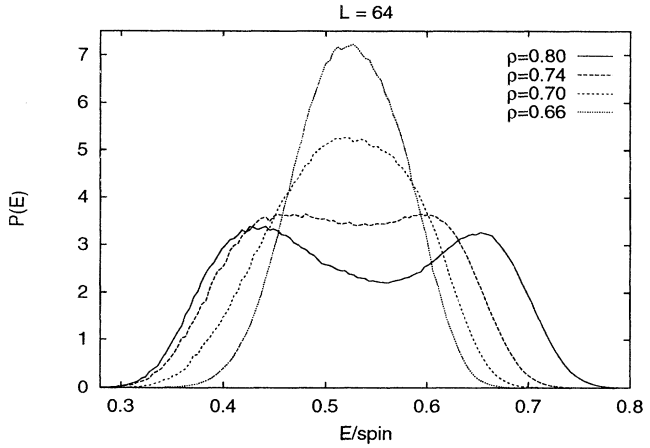

FIG. 5. Energy probability distributions $P(E)$ for different values of the asymmetry ρ and a lattice size $L = 64$ near the corresponding transition temperatures. The four distributions correspond to $\rho = 0.66$ and $T = 0.6810$, $\rho = 0.70$ and $T = 0.6967$, $\rho = 0.74$, and $T = 0.7132$, and $\rho = 0.80$ and $T = 0.7372$.

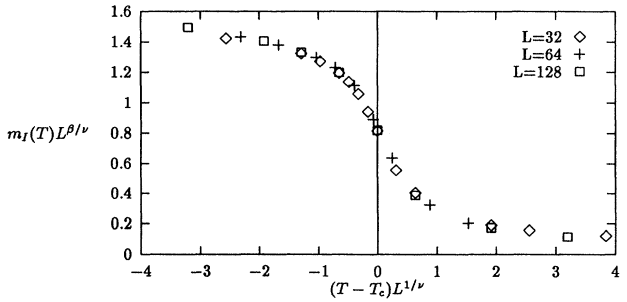

FIG. 6. Finite-size scaling analysis for $L = 32$, 64, 128, $\rho = 0.33$ and the lower transition temperature $T_c = 0.375$. The best agreement is obtained for $\beta = 0.115 \pm 0.01$ and $\nu = 1.0 \pm 0.1$.

TABLE I. Parameters of finite-size scaling analysis (see text).

	ρ	T_c^{32}	T_c^{64}	T_c^{128}	β	ν
m_I	0.33	0.38	0.376	0.375	0.115±0.01	1±0.1
m_P	0.33	0.581	0.577	0.574	0.085±0.01	0.9±0.1
m_I	0.5	0.558	0.555	0.553	0.12±0.01	1±0.1

β of the order parameter (magnetization) and of the exponent ν for the correlation length. The exact values are $\beta = 1/8 = 0.125$ and $\nu = 1$ for the Ising model, and $\beta = 1/9 = 0.111$ and $\nu = 5/6 = 0.8333$ for the $q = 3$ Potts model.[2] In Fig. 4 the order parameter is shown. The reduced data $m_I(T)L^{\beta/\nu}$ as a function of $(T - T_c)L^{1/\nu}$ is also shown in Fig. 6 for $\rho = 0.33$. The agreement is good, and the universal function is clearly seen.

The low-temperature transition is associated with the appearance of type y bonds, while the high-temperature transition is associated with the appearance of type z bonds (this will be inversed in the upper triangle $\rho > 1$). Therefore we have used the fluctuations of n_y and n_z as a second criterion to locate the transition lines. In particular the coincidence of the maxima of these two fluctuations determines point B. The corresponding curves for $\rho = 0.5$ and 0.8 are shown in Fig. 4.

The situation in the triangle $0 < v < u < 1$ is very reminiscent of that encountered in the (q_s, q_t) model[24] (see also Ref. 25) and in the Ashkin-Teller model.[26] The one-component six-state BMV model can be decomposed into a $(3, 2)$ two-component model: if we consider the six-state spin s as being composed of a two-state spin τ and a three-state spin σ according to the following rules,

s	0	1	2	3	4	5
τ	0	0	0	1	1	1
σ	0	1	2	0	1	2

we end up with the following single-bond Hamiltonian for the BMV model:

$$H(\tau\sigma,\tau'\sigma') = -(J_x - J_y + J_z)\,\delta_{\sigma\sigma'}\delta_{\tau\tau'} - (J_y - J_z)\,\delta_{\sigma\sigma'} - (-J_z)\,\delta_{\tau\tau'} - J_z - (J_y\delta_{\sigma,\sigma'+\tau'+1} + J_z\delta_{\sigma,\sigma'-\tau'-1})\,\delta_{\tau\tau'} \,. \tag{4.3}$$

The last term of Eq. (4.3) is due to the cyclic submatrices A of Eq. (2.2). Its form prevents the exact results of Au-Yang and Perk[13,14] from being applied to this model, but in the region $0 < v < u < 1$ of the phase diagram it turns out that one can neglect this term, since $\rho < 1$, and one recovers the Hamiltonian of the (q_s, q_t) model.[24,25,13] To summarize the phase diagram in the lower triangle $0 < v < u < 1$ of the ferromagnetic region, we have found a first-order transition line with equation $2u+3v = \sqrt{6}-1$ extending from the standard Potts transition point P to the point B of enhanced symmetry. For smaller values of ρ the model almost decouples into a three-state Potts model and an Ising model. Two critical lines separate a two-color phase from a disordered phase and from a one-color ferromagnetic phase.

This decoupling does not hold anymore in the upper triangle $0 \le u < v \le 1$ (or equivalently $\rho > 1$) of the ferromagnetic region. The results are summarized in Fig. 7, where the phase diagram in the region $(0 \le u \le 0.34, 0.28 \le v \le 0.80)$ is reproduced. The transition line near the transition point P of the standard model seems to diverge from the self-dual line Δ, even though it is a curve with slope $-2/3$ at the point P. The transition remains first order for $1 \le \rho \lesssim 1.6$. Our results are then consistent with a second-order critical line for $1.6 \lesssim \rho \lesssim 2.0$. For $\rho \gtrsim 2$ we have found two transitions, and another phase occurs between the ordered low-temperature phase and the disordered high-temperature phase. Note that point B', where the transition line splits into two branches, is significantly far from the self-dual line Δ. As an example, the specific heat and magnetizations for two different values of the asymmetry ρ are shown on Fig. 8. The low-temperature transition is clearly seen, but the high-temperature transition is much weaker. We had to go to sizes as large as $L = 128$ and perform extensive averages to see the size effects convincingly. The intermediary phase is not easy to characterize.

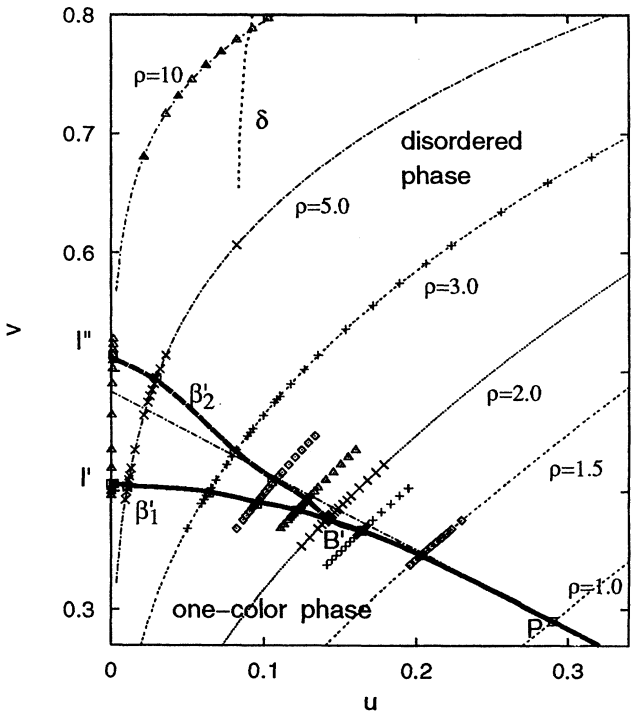

FIG. 7. A part of the ferromagnetic region of the phase diagram of the BMV model with simulation points and lines of constant asymmetry (see text).

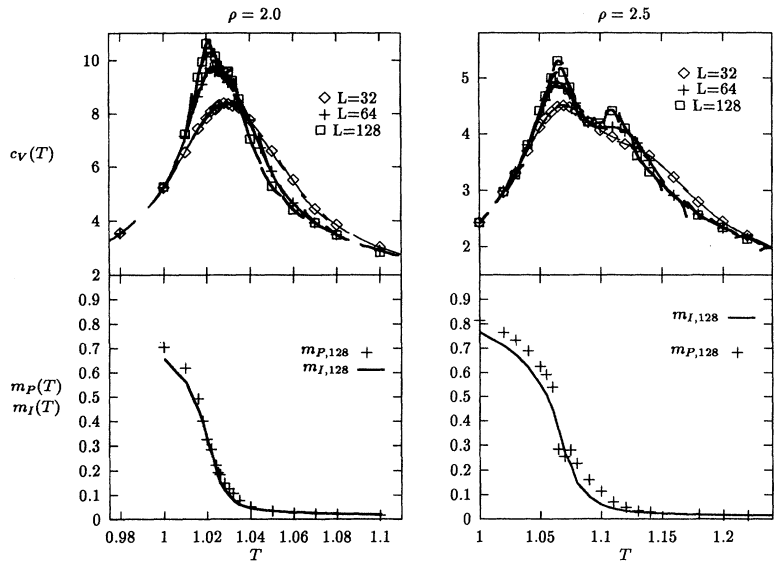

FIG. 8. Specific heat and the order parameters as functions of the temperature for $\rho = 2.0$ and $\rho = 2.5$ (see text). For the specific heat the lines were obtained by extrapolation with the histogram method, for the order parameters they are only a guide to the eyes.

We checked by inspection that typical configurations in this phase have no obvious structure (as stripes). The full comprehension of this phase deserves more work and especially the computation of correlation functions, but we suggest that this phase is a trace of the floating phase present in the isotropic three-state chiral Potts model;[12] the submatrix A of W (2.2) is indeed the generic matrix of the general three-state chiral Potts model where floating phases have been found. The additional degrees of freedom present in the BMV model could prevent the stabilization of the floating phase. Note also that the intermediary phase does not extend into the nonferromagnetic region, by contrast with the intermediary phase in the $u > v$ ferromagnetic region.

V. NONFERROMAGNETIC REGION

The nonferromagnetic regions of the phase diagram are characterized by low-energy physics. In contrast with the ferromagnetic region (where x is larger than both y and z) the ground state in the nonferromagnetic regions is highly degenerated. Two cases have to be considered depending on whether y or z is the largest of the three weights x, y, and z.

If y is larger than x and z, then the analysis of the ground state and the evaluation of the residual entropy can be done. The simple inspection of all possible four-spin plaquettes with only type y bonds shows that the spins of the upper-right and the lower-left corners are always of the same color (arrows are oriented from the left to the right and from the top to the bottom). Therefore the states of lowest energy will be composed of diagonal stripes of spins of the same color. A ground state will be determined by the color of each of the L diagonal stripes of unit width running accross the sample. To construct a ground state we start by choosing the color of a first diagonal d_0. There are six possible choices. We then have to choose the color of the first adjacent diagonal stripe d_1. The form of the Boltzman weight matrix (2.2) imposes choosing one among two possible colors. For example, if the color of d_0 is 0, then the color of d_1 can only be 1 or 3. Applying $L-1$ times the same procedure completely determines a ground state. Taking into ac-

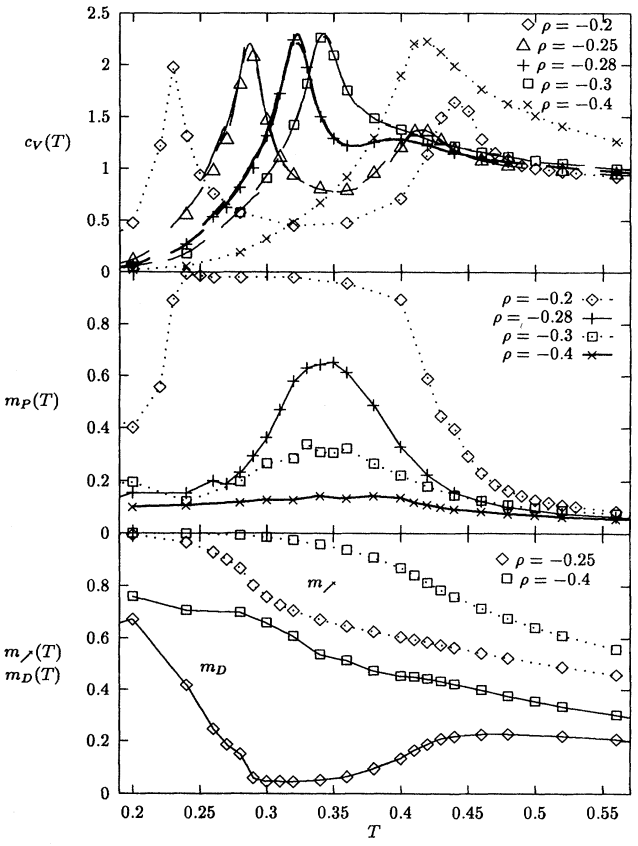

FIG. 9. Specific heat, magnetizations and next neighbor correlations as functions of temperature for different values of the asymmetry in the mixed region $u > v$.

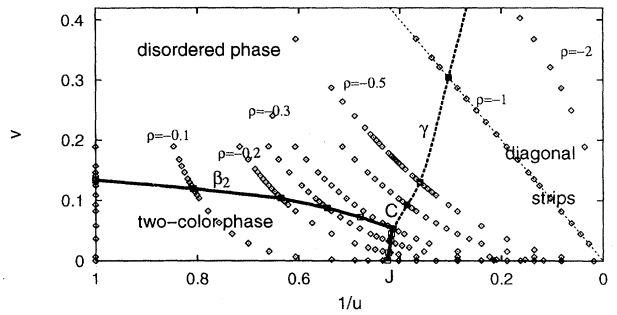

FIG. 10. A part of the mixed region $u > v$ of the phase diagram with simulation points (see text).

count the periodic boundary conditions, it appears that it is possible to construct states with only type y bonds, which means that there is no frustration. Moreover, there are exactly 2^L such states, and therefore the residual entropy $\ln 2/\sqrt{N}$ is vanishing in the thermodynamic limit. It is also possible to estimate the energy barriers between two ground states: using a single spin-flip algorithm the cost in energy to go from one ground state to another one is independent of the size L of the sample, and therefore all the ground states are "close" to each other, but note that the optimum path in configurational space to reach a given ground state from a random one is very constrainted. The band structure of a configuration can be quantitatively characterized by the following quantities:

$$n_{\searrow} = \frac{1}{N}\sum_{i,j=1}^{L} \delta(\sigma_{i,j}, \sigma_{i+1,j+1}) \ , \tag{5.1}$$

$$n_{\nearrow} = \frac{1}{N}\sum_{i,j=1}^{L} \delta(\sigma_{i,j+1}, \sigma_{i+1,j}) \ , \tag{5.2}$$

$$m_D = \langle |n_{\searrow} - n_{\nearrow}| \rangle \ . \tag{5.3}$$

The quantity $n_{\nearrow}$ measures the correlation in the direction of the stripes (lower-left corner to upper-right corner), while $n_{\searrow}$ measures the correlation between adjacent stripes. A value of m_D close to unity indicates that the configuration has a band structure. Figure 9 shows the behavior of these quantities as functions of the temperature for different values of the asymmetry ρ. The specific heat is also shown. The location of the iso-ρ lines in this part of the phase diagram can be found in Fig. 10. Figure 11(a) shows a typical configuration of the diagonal stripe phase. When $\rho \lesssim -0.3$ our results show that the system goes from the disordered phase at high temperature to the ordered striped phase at low temperature without undergoing a phase transition. The specific heat presents a broad maximum without size effects (see Fig. 9). The broken line γ in the phase diagram (Fig. 2) corresponds to the locus of this maximum. Conversely when $-0.3 \lesssim \rho < 0$ the specific heat as a function of temperature presents two maxima becoming sharper when the lattice size is increased. The behavior of the magnetizations and of the two quantities n_y and n_z introduced in the preceding section shows that the intermediary phase is a two-color phase. The high-temperature transition line is the continuation of the line β_2 from the ferromagnetic region, and the two-color phase is also the same as the two-color phase of the ferromagnetic region. The low-temperature transition points define a line CJ, which, according to our results, is a line of second-order transition.

If now z is greater than both x and y, there is also no frustration in the ground states. Their number is much greater than in the preceding case so that the residual entropy per spin is nonvanishing in the thermodynamic limit, even though we can only give an approximate expression of it. In principal, the same procedure as in the case where $\max(x, y, z) = y$ can be carried out to construct a ground state. The system is now less constrained: spins s of the upper-right corner and spin s' of the lower-left corner of a plaquette need not to be of the same color any longer. Instead, if s has a given color, then s' can have up to two colors. Figure 11(b) shows a typical low-temperature configuration. For an enumeration of the ground states one has to proceed now in diagonals from the upper-left to the lower-right, and one finds that the number of ground states behaves like $3(2^{\alpha})^N$, where N is the number of sites and α is a constant of about $1/2$. So we get a finite value for the residual entropy per spin at zero temperature. Figure 12 presents the specific heat as a function of temperature along iso-ρ lines. The maximum of the specific heat shows no size dependence. The locus of these maxima has been traced as the dotted line δ in the phase diagram (Fig. 2). The mean-field

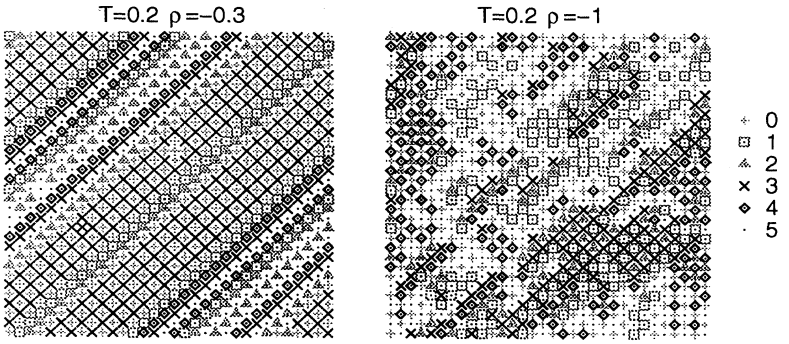

FIG. 11. (a) A typical configuration for $T = 0.24$ and $\rho = -0.3$ in the mixed region $u > v$. (b) A typical configuration for $T = 0.2$ and $\rho = -1$ in the mixed region $u < v$.

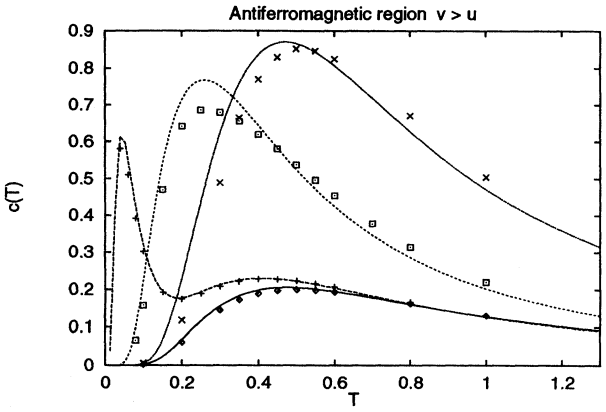

FIG. 12. Specific heat as a function of temperature in the $v > u$ antiferromagnetic region. The points are the results of the simulation. The lines are the mean-field specific heat with the corresponding parameters: $\Diamond$ $\rho = 1.0$, $+$ $\rho = 0.9$, $\Box$ $\rho = 0.5$, and $\times$ $\rho = -0.2$.

specific heat is also shown in the same figure. The agreement is surprisingly good, showing that the effect of the loops of the lattice is irrelevant in this region of the phase diagram and that there is no collective effect.

VI. CONCLUSION

We have analyzed the phase diagram of the isotropic BMV model by means of Monte Carlo simulations. The resulting phase diagram is shown in Fig. 2. The chirality of the model seems to play no special role in the ferromagnetic region. In a part of this region the behavior of the model can be explained by the coupling of an Ising model with a three-state standard Potts model as the (q_s, q_t) model.[25] We also have proposed an exact expression for the transition line PB. In the region $u > 1$ and $u > v$, the low temperature phase is ordered in diagonal stripes, which can be deduced from the Boltzmann weight matrix (2.2). In the region $v > 1$ and $v > u$ the model seems to be well approximated by the Bethe lattice as a mean-field approximation.

ACKNOWLEDGMENTS

We thank J.M. Maillard and G. Rollet for stimulating discussions.

* Electronic address: hmeyer@crtbt.polycnrs-gre.fr dauriac@crtbt.polycnrs-gre.fr

[1] R.B. Potts, Proc. Comb. Philos. Soc. **48**, 106 (1952).
[2] F.Y. Wu, Rev. Mod. Phys. **54**, 235 (1982).
[3] *The Monte Carlo Method in Condensed Matter Physics*, Topics in Applied Physics Vol. 71, edited by K. Binder (Springer-Verlag, Berlin, 1992).
[4] R.J. Baxter, *Exactly Solved Models in Statistical Mechanics* (Academic, London, 1982).
[5] W. Selke, Phys. Rep. **170**, 213 (1988); W. Selke, in *Phase Transitions and Critical Phenomena*, edited by C. Domb and J.L. Lebowitz (Academic, New York, 1992), Vol. 15.
[6] H. Au-Yang and J.H.H. Perk, Physica A **177**, 139 (1991).
[7] P.A. Pearce and H.L. Scott, Jr., J. Chem. Phys. **77**, 951 (1982).
[8] D. Kim, P.M. Levy, and J.J. Sudano, Phys. Rev. B **13**, 2054 (1976); B **12**, 989 (1975).
[9] H. Au-Yang, B.M. Mc Coy, J.H.H. Perk, S. Tang, and M.L. Yan, Phys. Lett. A **123**, 219 (1987).
[10] B.M. Mc Coy, J.H.H. Perk, S. Tang, and C.H. Sah, Phys. Lett. A **125**, 9 (1987).
[11] R.J. Baxter, J.H.H. Perk, and H. Au-Yang, Phys. Lett. A **128**, 138 (1988).
[12] J.C. Anglès d'Auriac, D. Hansel, and J.M. Maillard, J. Phys. A **22**, 2577 (1989).
[13] H. Au-Yang and J.H.H. Perk, Intern. J. Mod. Phys. A **7**, 1025 (1992).
[14] H. Au-Yang and J.H.H. Perk, Intern. J. Mod. Phys. A **7**, 1007 (1992).
[15] J.M. Maillard, J. Phys. (Paris) **46**, 329 (1985).
[16] M.P. Bellon, J-M. Maillard, and C-M. Viallet, Phys. Lett. A **159**, 221 (1991).
[17] M.P. Bellon, J-M. Maillard, and C-M. Viallet, Phys. Lett. A **159**, 233 (1991).
[18] M.P. Bellon, J-M. Maillard, and C-M. Viallet, Phys. Lett. A **157**, 343 (1991).
[19] M.P. Bellon, J-M. Maillard, and C-M. Viallet, Phys. Rev. Lett. **67**, 1373 (1991).
[20] H. Meyer, J.C. Anglès d'Auriac, J.M. Maillard, and G. Rollet, Physica A **209**, 223 (1994).
[21] A.B. Zamolodchikov and M.I. Monarstyrskii, Sov. Phys. JETP **50**, 167 (1979).
[22] M. Kardar, Phys. Rev. B **26**, 2693 (1982)
[23] A.M. Ferrenberg and R.H. Swendson, Phys. Rev. Lett. **61**, 2635 (1988).
[24] E. Domany and E.K. Riedel, Phys. Rev. B **19**, 5817 (1979); J. Appl. Phys. **49**, 1315 (1978).
[25] M.P.M. den Nijs, Physica A **95**, 449 (1979).
[26] J. Ashkin and E. Teller, Phys. Rev. **64**, 178 (1943).